Ringdown Electromechanical Oscillations Analysis Through the Interpolated DFT Algorithm

Daniel Belega
Department of Measurements and Optical Electronics
Politehnica University Timisoara
Timisoara, Romania
daniel.belega@upt.ro

David Macii, Dario Petri
Department of Industrial Engineering
University of Trento
Trento, Italy
{david.macii, dario.petri}@unitn.it

This paper proposes the analysis of the ringdown electromechanical oscillations occurring in power systems through the two-point Interpolated Discrete Fourier Transform (IpDFT) algorithm for damped sinusoids. In particular, the frequency and the damping factor of the modes of interest are estimated. The accuracy of the proposed algorithm is compared with that of a rather standard technique, i.e. the Prony algorithm, in order to evaluate the main advantages and disadvantages of either approach under different operating conditions. The results of several simulations show that the IpDFT algorithm is preferable when the signal-to-noise ratio is low or moderate, whereas the Prony algorithm is more robust to spectral interference when the oscillating modes are closely spaced in frequency.

I. Introduction

During the transfer of power between power networks, electromechanical oscillations may occur [1]-[5]. To ensure a safe operation of the whole network, Wide Area Monitoring Systems (WAMS) are employed, which exploit also data provided by Phasor Measurement Units (PMUs) [2], [3]. Electromechanical oscillations proprieties depend on the characteristics of both the generators and the network. These oscillations are classified as local modes (which involve units of a given plant swinging against each other or against the rest of the system) and inter-area modes (which involve large groups of generators) [1], [3], [4]. Depending on the kind of event causing oscillations, ambient, ringdown (i.e., transient), or forced responses can be observed [3]-[5]. Both ambient and ringdown responses can be accurately modeled as linear combinations of damped sinusoids, corresponding to the modes of the power system. However, while ambient responses are typically related to customary random load variations, ringdown oscillations are due to sudden events. Unlike ambient responses, they exhibit shorter duration and larger magnitude. For both types of electromechanical oscillations, different algorithms have been proposed in the literature to estimate the frequency, the damping factor, the amplitude and the initial phase of each mode. Frequency and damping factor are estimated by means of parametric algorithms such as the Prony method [1], [6]-[10], the Kalman filter [2], [11], the Matrix Pencil algorithm [10], [12], [13], the Hilbert-Huang transform [10], [14], [15], the Taylor-Fourier algorithm [16], the Eigensystem Realization Algorithm (ERA) [17], or the Dynamic Mode Decomposition algorithm [1]. However, the Prony method is the most widely used even if it exhibits a high sensitivity to wideband noise, which is mitigated by increasing the order of the underlying signal model [2], [5], [8].

On the other hand, the frequency and the damping factor of a real-valued damped sinusoid can be accurately estimated by means of the Interpolated Discrete Fourier Transform (IpDFT) approach for damped sinusoids [18]-[20]. This approach is very simple to implement, and the related algorithms are accurate and exhibit low computational complexity. Thus, the IpDFT approach can be advantageously employed in real-time applications even if low-cost processing platforms are adopted. However, to the best of the Authors' knowledge, it has not been employed in the analysis of ringdown electromechanical oscillations yet. The aim of this paper is to investigate the accuracy of the two-point IpDFT algorithm based on a Maximum Sidelobe Decay (MSD) window when estimating the frequency and the damping factor of electromechanical oscillation modes. Quite importantly, the MSD windows have been chosen since they exhibit the highest sidelobe decaying rate among all the cosine-class windows with the same number of coefficients [21], thus providing an optimal long-range reduction of the spectral interference between oscillation modes. Moreover, when an MSD window is used, the IpDFT frequency and the damping factor estimates are provided by very simple expressions [19], [20].

II. The Two-Point IpDFT Algorithm

Let us consider a sum of K damped real-valued sinusoids (namely the modes of the system), modelled as [2]:

$$x(m) = \sum_{k=1}^{K} A_k e^{-\frac{\alpha_k}{f_s} m} \cos\left(2\pi \frac{f_k}{f_s} m + \phi_k\right), \quad m = 0, 1, \ldots, M-1 \tag{1}$$

where A_k, f_k, ϕ_k, and α_k are the amplitude, the frequency, the initial phase, and the damping factor of the k-th mode; f_s is the sampling rate and M is the record length. The duration of the observation interval is equal to M/f_s. Since the frequencies of electromechanical oscillations are usually in range 0.1 - 2 Hz, observation interval durations approximately equal to or greater than 5 s are often considered in the literature [2], [16]. However, the use of shorter windows enables faster estimates and better responsinveness.

The ratio between the frequency of the k-th mode f_k and the sampling rate f_s can be expressed as:

$$\frac{f_k}{f_s} \stackrel{\text{def}}{=} \frac{\lambda_k}{M} = \frac{l_k + \delta_k}{M}, \tag{2}$$

where $\lambda_k = l_k + \delta_k$ is the normalized frequency (expressed in bins), which also represents the number of observed cycles of the k-th mode; l_k and δ_k ($-0.5 \leq \delta_k < 0.5$) are the closest integer and the fractional parts of λ_k, respectively.

The damping ratio ζ_k of the kth mode is finally defined as [2]:

$$\zeta_k(\%) = -\frac{\alpha_k}{\sqrt{\alpha_k^2+(2\pi f_k)^2}} \cdot 100, \quad (3)$$

To reduce the effect of the image component and the other spectral components on the estimated parameters of the mode of interest, the analyzed signal is weighted by a suitable window $w(m)$, so obtaining the windowed signal $x_w(m) = x(m) \cdot w(m)$. In the following, an H-term MSD window is adopted, which is defined as:

$$w(m) = \sum_{h=0}^{H-1}(-1)^h a_h \cos\left(\frac{2\pi hm}{M}\right), \quad m = 0, 1, \ldots, M-1 \quad (4)$$

where $H \geq 2$ is the number of window terms and a_h are the window coefficients, equal to $a_0 = \frac{C_{2H-2}^{H-1}}{2^{2H-2}}$ or $a_h = \frac{C_{2H-2}^{H-1-h}}{2^{2H-3}}$, $h = 1, 2, \ldots, H-1$, with $C_n^q = \frac{n!}{(n-q)! \cdot q!}$ [19].

To assure that the interference between different spectral components is small, the following constraint is assumed [22]-[24]:

$$\min_{\substack{1 \leq i,j \leq K \\ i \neq j}} |f_i - f_j| > 2H\frac{f_s}{M}, \quad (5)$$

which results in the following lower bound on the observation interval length:

$$\frac{M}{f_s} > \frac{2H}{\min_{\substack{1 \leq i,j \leq K \\ i \neq j}} |f_i - f_j|}. \quad (6)$$

Under such constraint, the two-point IpDFT algorithm based on the H-term MSD window returns accurate estimates of the k-th mode frequency and damping factor $\hat{\alpha}_k$, if the following expressions are used [20]:

$$\hat{f}_k = s_k \frac{f_s}{M} \operatorname{Re}\left\{\frac{H\rho_k + H - 1}{\rho_k - 1}\right\}, \quad (7a)$$

$$\hat{\alpha}_k = s_k \frac{2\pi f_s}{M} \operatorname{Im}\left\{\frac{H\rho_k + H - 1}{\rho_k - 1}\right\}, \quad (7b)$$

where:

$$\rho_k = \frac{X_w(l_k+s)}{X_w(l_k)}, \; s_k = \operatorname{sign}(|X_w(l_k+1)| - |X_w(l_k-1)|),$$

$X_w(\cdot)$ is the DFT of the windowed signal $x_w(m)$, Re{·} and Im{·} are the real and the imaginary part operators, and sign(·) is the sign function.

When the analyzed signal $x(m)$ is affected by additive white Gaussian noise with zero mean and variance σ_n^2, the biases of the estimators (7a)-(7b) are negligible, while the related variances are [20]:

$$\sigma_{\hat{f}_k}^2 = 4\pi^2\sigma_{\hat{\alpha}_k}^2 \cong$$

$$\frac{4\pi^2 f_s^2 C_{4H-4}^{2H-2}}{[(2H-1)!\,]^2 \cdot M^3 \cdot SNR_k} \frac{(\delta_k^2 + \alpha_k^2)[(\delta_k - s_k \cdot H)^2 + \alpha_k^2]}{1 - 2e^{-2\pi\alpha_k}cos(2\pi\delta_k) + e^{-4\pi\alpha_k}}$$

$$\frac{2(4H-3)(\delta_k^2 - s_k \cdot \delta_k + \alpha_k^2) + 2H^2 - 1}{2H-1}$$

$$\times \prod_{h=1}^{H-1}[(\alpha_k^2 - \delta_k^2 + h^2)^2 + 4\alpha_k^2\delta_k^2], \quad (8)$$

where SNR_k is the Signal-to-Noise Ratio of the k-th mode, defined as $SNR_k \triangleq^{\text{def}} A_k^2/(2\sigma_n^2)$.

III. ACCURACY COMPARISON

In this Section the accuracy of the frequency and the damping factor estimates provided by the IpDFT and the Prony algorithms are compared in different scenarios.

• *Case #1*

Firstly, the behavior of the Southern/Southeastern Brazilian power system [3] is analyzed as a function of the *SNR* in the range [10, 70] dB (with a step of 2 dB), when a single inter-area mode with frequency f = 0.8328 Hz and damping ratio ζ = 6.93% occurs. The amplitude of the damped signal is A = 1 p.u.. As suggested in [2], the sampling rate is f_s = 10 Hz, and the observation interval duration is 5 s, which leads to M = 50 analyzed samples. For each *SNR* value 10,000 runs of M samples each are considered. The initial signal phase is chosen at random in the interval [0, 2π) rad. Fig. 1 shows the analyzed signal in the time domain when the initial phase is 0 rad and *SNR* = 40 dB.

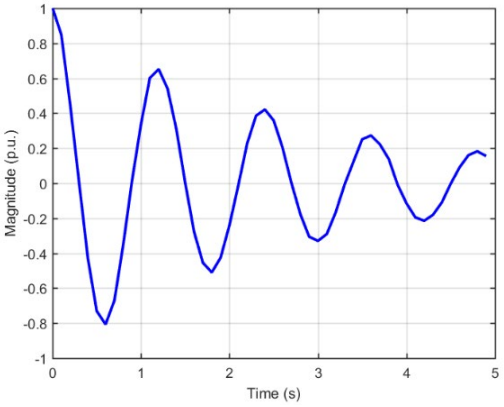

Fig. 1. Case #1: time behavior of the inter-area signal modelling a power system oscillation characterized by f = 0.8323 Hz and ζ = 6.93%. The initial signal phase is set to 0 rad and the *SNR* is 40 dB.

In the IpDFT algorithm the two-term MSD (or Hann) window is used, while a fourth-order model is chosen in the Prony algorithm. Figs. 2 and 3 show the mean and the standard deviation of the frequencies and the damping ratio estimates returned by the Prony and the IpDFT algorithms as a function of the *SNR*. Observe that when the *SNR* is lower than about 30 dB, the IpDFT algorithm outperforms the Prony algorithm. When the *SNR* is higher than about 55 dB instead, the standard deviation values of both IpDFT estimates become higher than those returned by the Prony algorithm. Also, this performance gap increases as the *SNR* grows. This behavior is due to the contribution of the fundamental image component to the IpDFT parameter estimates, which prevails over wideband noise for high *SNR* values. However, for both estimated parameters, the standard deviation is much smaller than the mean when the *SNR* is greater than about 55 dB. A possible way to reduce the detrimental contribution of the image component is to increase the number of observed signal cycles, as shown in Fig. 4, where the observation interval duration is 10 s.

Simulations showed that behaviors like those depicted in Figs. 2-4 as long as ζ is smaller than about 9%. Conversely, when 9% < ζ < 50%, the mean of the estimated parameters behaves similarly to Figs.2-4, while the Prony estimates exhibit smaller standard deviations.

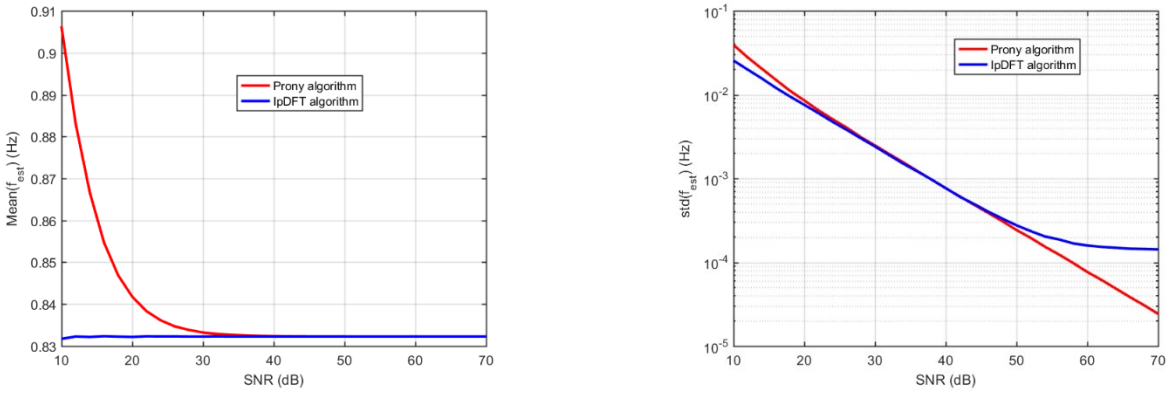

Fig. 2. Case #1: mean (a) and standard deviation (b) of the inter-area signal frequency estimates provided by the Prony and the IpDFT algorithms versus *SNR*. The IpDFT algorithm relies on the Hann window, while the Prony algorithm is based on a fourth-order model. The sampling rate f_s is 10 Hz and the observation interval duration is 5 s. All the curves result from 10,000 runs of M = 50 samples each with the signal initial phase chosen at random.

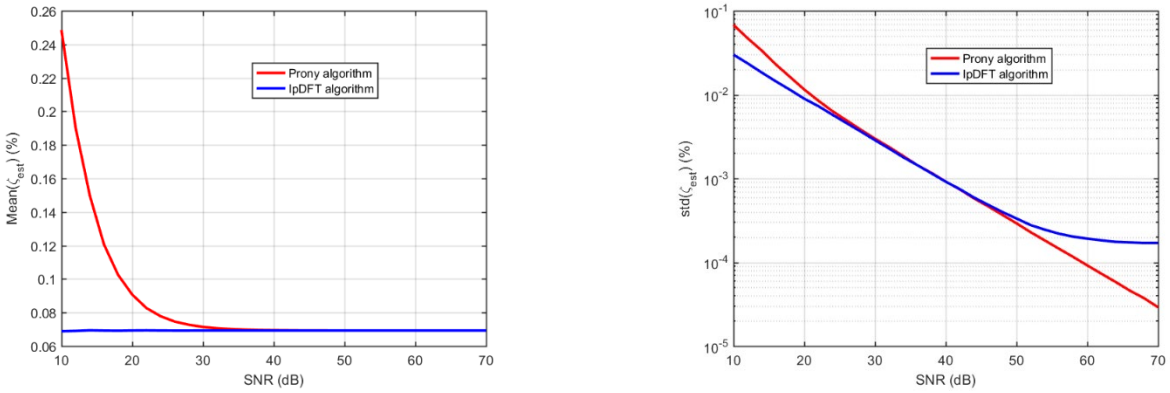

Fig. 3. Case #1: mean (a) and standard deviation (b) of the inter-area signal damping ratio estimates provided by the Prony and the IpDFT algorithms versus *SNR*. The IpDFT algorithm relies on the Hann window, while the Prony algorithm is based on a fourth-order model. The sampling rate f_s is 10 Hz and the observation interval duration is 5 s. All the curves result from 10,000 runs of M = 50 samples each with the signal initial phase chosen at random.

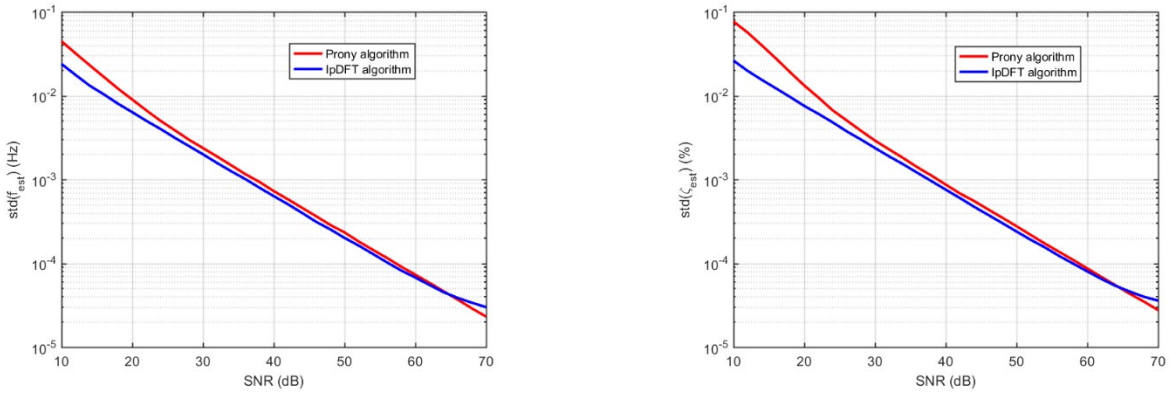

Fig. 4. Case #1: standard deviation of the inter-area signal frequency (a) and damping ratio (b) estimates provided by the Prony and the IpDFT algorithms versus *SNR*. The IpDFT algorithm relies on the Hann window, while the Prony algorithm is based on a fourth-order model. The sampling rate f_s is 10 Hz and the observation interval duration is 10 s. All the curves result from 10,000 runs of M = 100 samples each with the signal initial phase chosen at random.

• *Case #2*

In this case, three modes, characterized by the following parameters are considered [2]:

Mode 1: A_1 = 1.5 p.u, f_1 = 0.5 Hz, α_1 = 0.1 (ζ_1 = 3.18%),

Mode 2: A_2 = 0.5 p.u, f_2 = 0.9 Hz, α_2 = 0.3 (ζ_2 = 5.30%),

Mode 3: A_3 = 0.7 p.u, f_3 = 1.5 Hz, α_3 = 0.5 (ζ_3 = 5.30%).

The sampling rate f_s is 10 Hz, and the observation interval duration is 10 s. In this case, constraint (6) (which should ensure accurate IpDFT estimates) is fulfilled for all modes.

Fig. 5 shows each mode and their summation as a function of time when the initial phase of all modes is set to 0 rad. Clearly, mode 1 dominates over the others.

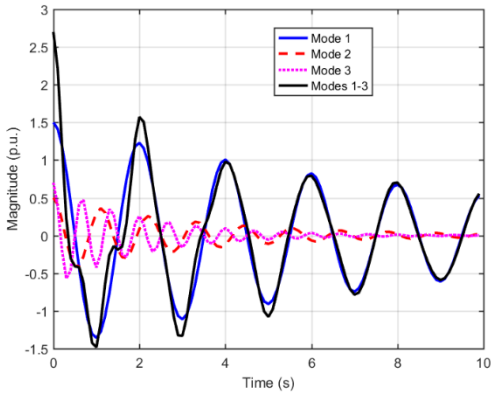

Fig. 5. Case #2: individual modes as a function of time and aggregated waveform. The initial phase of all modes is set to 0 rad.

Fig. 6 shows the mean and the standard deviation of the modes' frequency estimated by the Prony and the IpDFT algorithms, respectively, versus the *SNR* of the dominating mode SNR_1, which ranges from 10 dB to 70 dB with steps of 2 dB. In this case study, a 12-order model is used in the Prony algorithm. For each SNR_1 value, 10,000 runs of M = 100 samples each are considered and the initial phases of all components are chosen at random in the interval [0, 2π) rad. The trends of the damping ratio estimates are very similar to those shown in Fig. 6 for the frequency estimates;so that they are not reported.

Fig. 6 shows that the IpDFT algorithm outperforms the Prony method when the *SNR* is lower than about 40 dB. Conversely, for higher *SNR* values both algorithms return almost the same mean frequency value. However, the Prony method ensures a smaller estimator standard deviation since the estimates returned by the IpDFT algorithm are affected by the spectral interference due to the image component and the other tones. Anyway, both algorithms provide very accurate parameter estimates, especially for the dominant mode.

The accuracy of both algorithms is further analyzed when two modes exhibit very close frequencies, i.e., when constraint (6) is not fulfilled. This is the case of modes 1 and 2 when mode 2 frequency is f_2 = 0.6 Hz [2]. In this case the distance between the two spectral components is 1 bin only. The results obtained considering the same simulation conditions as in Fig. 6 are reported in Fig. 7. Figs. 7(b) and (e) show that the IpDFT frequency estimates of mode 2 are not accurate due to the strong spectral interference of mode 1. In particular, the estimated mean value coincides with the mode 1 frequency and the estimator standard deviation is high. However, the frequency of modes 1 and 3 is accurately estimated. Compared with Fig. 6(a), Fig. 7(a) shows that the mean value of mode 1 frequency estimates exhibits significant variations due to the interference of mode 2. This fact is confirmed by Fig. 7(d), which shows that the standard deviation of the IpDFT frequency estimates is almost independent of the SNR_1 values. The Prony algorithm accurately estimates the frequencies of each mode when SNR_1 is greater than about 60 dB for mode 1, 50 dB for mode 2, and 40 dB for mode 3, respectively. Compared with Fig. 6, Fig. 7 shows that modes 1 and 2 interference increases the SNR_1 threshold above which the Prony algorithm returns accurate mode 1 and mode 2 frequency estimates.

Very often, both fast and accurate estimates of the dominant mode parameters are of interest [2]. Thus, an observation interval duration of 3 s is assumed and the mean and the standard deviation of the frequency estimates returned by both considered algorithms are reported in Fig. 8. Observe that, in the considered testing conditions, the contributions of mode 1 and mode 2 are merged into a single spectrum peak and cannot be analyzed individually.

Fig. 8 shows that the estimation bias of the IpDFT algorithm is lower than the Prony algorithm's one. Conversely, the frequency estimates of both algorithms exhibit almost the same standard deviations when SNR_1 is smaller than about 40 dB, while the Prony algorithm ensures smaller standard deviations for higher SNR_1 values. Indeed, the IpDFT estimates are affected by the spectral interference of different spectral components, which increases over shorter observation intervals.

The processing time of a A MATLAB implementation of the considered algorithms is analyzed in Table I. To measure such processing times, the function *timeit*(·) was used and the integer part of the number of observed cycles of each mode was assumed to be known *a priori*. The MATLAB function *fft*(·) function wasemployed in the IpDFT algorithm. A laptop computer equipped with a Core i7-1165G7 processor running at 2.80 GHz, with 16 GB RAM, and Windows 10 operating system was employed. Table I shows the average a processing time of either algorithm obtained when processing 1000 runs for different values of *M*..

TABLE I. PROCESSING TIME OF THE IPDFT AND THE PRONY ALGORITHMS.

Signal	***# samples M***	***Algorithm processing time (μs)***	
		Prony	***IpDFT***
Case #1	50	40.89	6.17
Case #1	100	42.45	7.68
Case #2	100	83.34	9.02

As we can see, the processing time of the IpDFT algorithm is much smaller than the Prony algorithm's one.

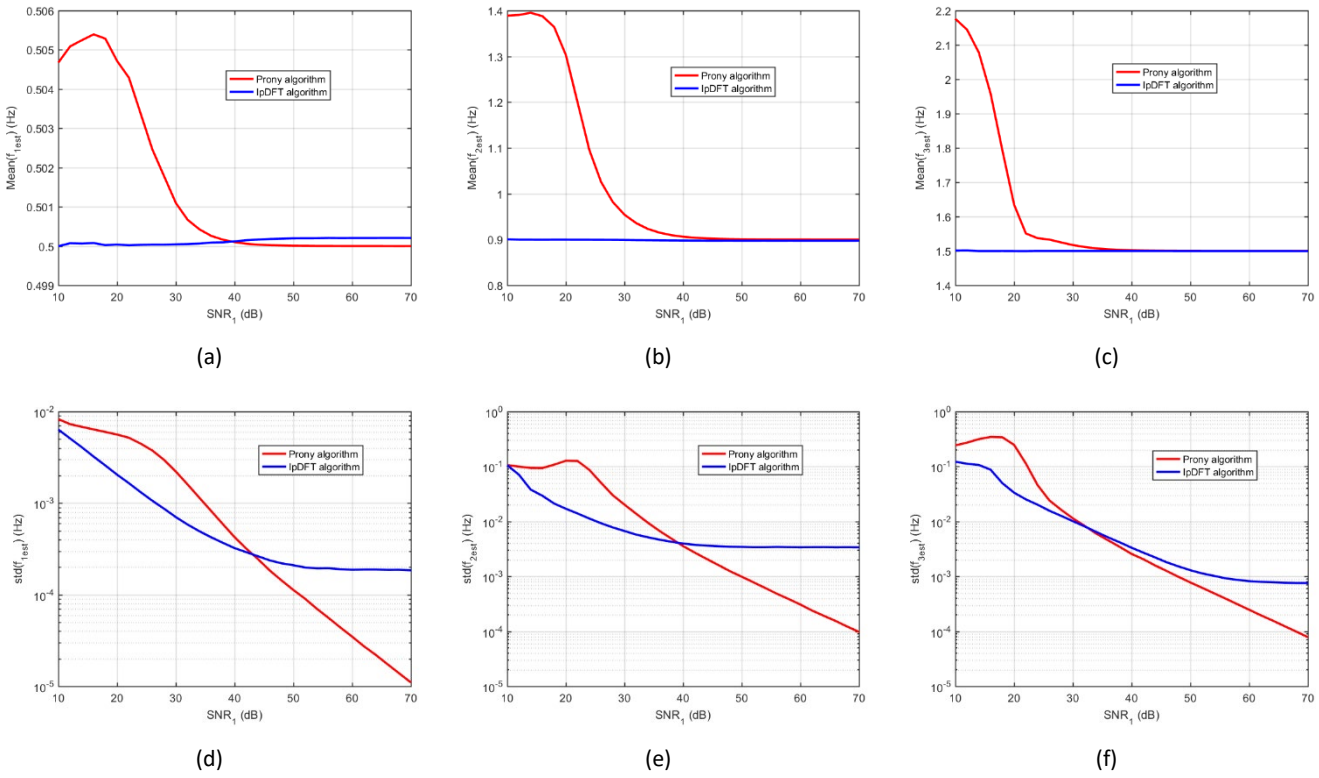

Fig. 6. Case #2: mean (a) – (c) and standard deviation (d) – (f) of different mode frequencies estimated by the Prony and the IpDFT algorithms versus SNR_1. The IpDFT algorithm relies on the Hann window, while the Prony algorithm is based on a 12th order model. The sampling rate f_s is 10 Hz and the observation interval duration is 10 s. All the curves result from 10,000 runs of M = 100 samples each with the initial phase of all components chosen at random.

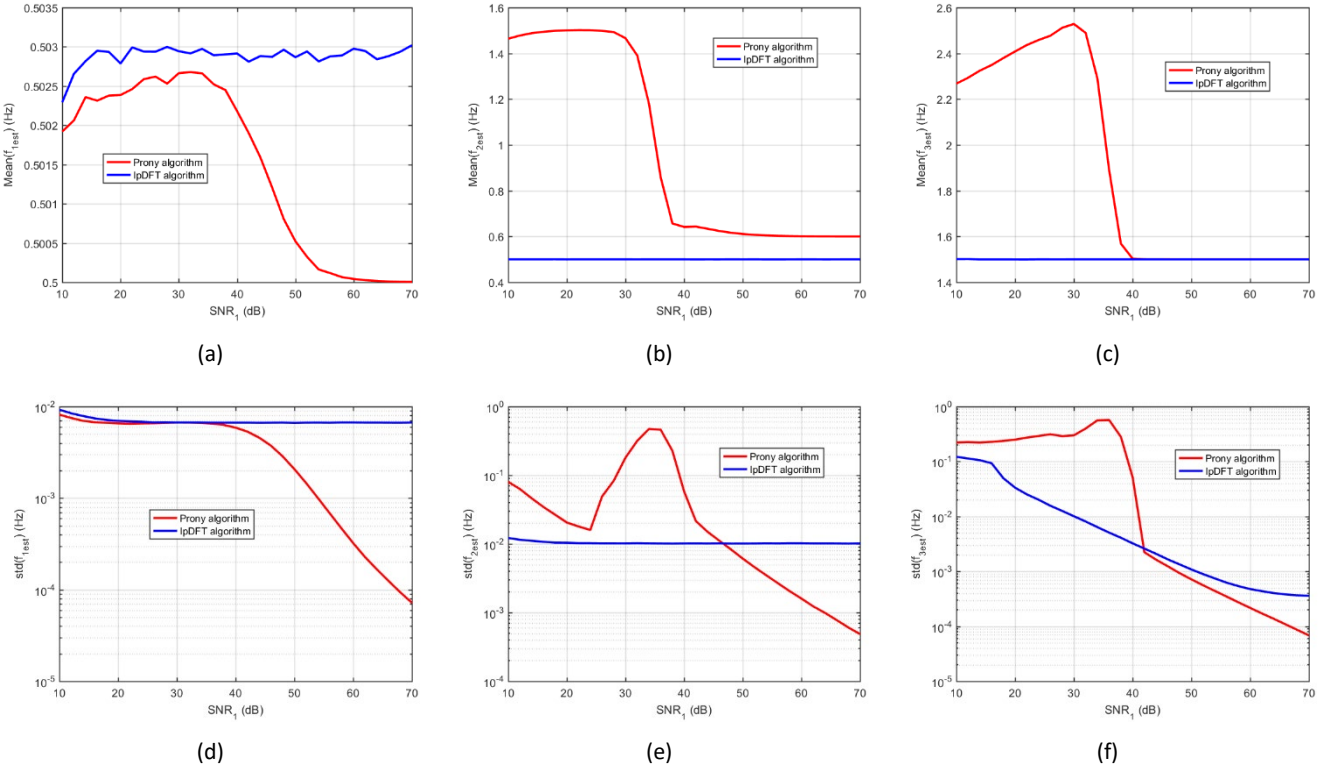

Fig. 7. Case #2 with f_2 = 0.6 Hz: mean (a) – (c) and standard deviation (d) – (f) of different mode frequencies estimated by the Prony and the IpDFT algorithms versus SNR_1. The IpDFT algorithm relies on the Hann window, while the Prony algorithm is based on a 12th order model. The sampling rate f_s is 10 Hz and the observation interval duration is 10 s. All the curves result from 10,000 runs of M = 100 samples each with the initial phase of all components chosen at random.

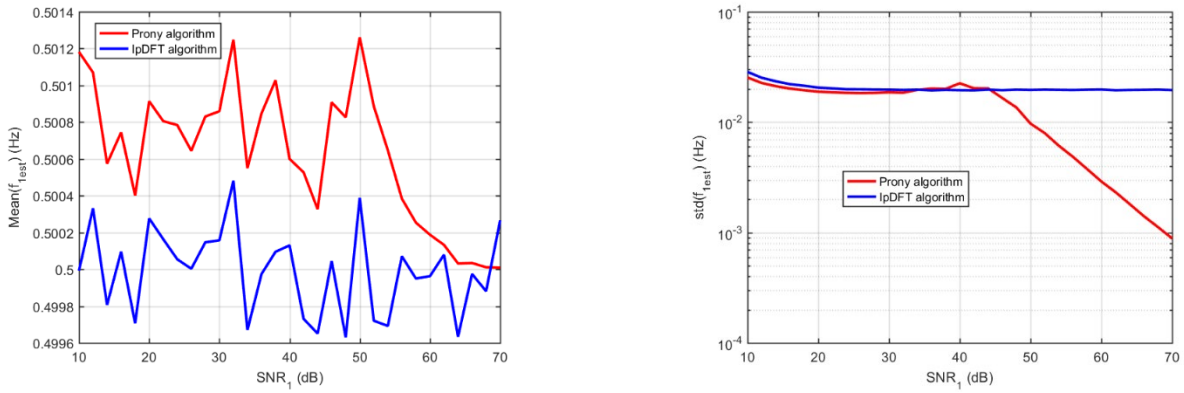

(a) (b)

Fig. 8. Case #2 with f_2 = 0.6 Hz: mean (a) and standard deviation (b) of the dominant mode frequency estimated by the Prony and the IpDFT algorithms versus SNR_1. The IpDFT algorithm relies on the Hann window, while the Prony algorithm is based on a 12th order model. The sampling rate f_s is 10 Hz and the observation interval duration is 3 s. All the curves result from 10,000 runs of M = 30 samples each with the initial phase of all components chosen at random.

IV. Conclusions

In this paper the two-point IpDFT algorithm for damped sinusoids is used to estimate the modes' parameters of the ringdown electromechanical oscillations occurring in power systems. The accuracy of the IpDFT algorithm is compared with the accuracy of the widely adopted Prony algorithm. The reported simulation results show that the IpDFT algorithm is more robust to wideband noise and provides almost the same accuracy as the Prony algorithm. Conversely, the Prony algorithm exhibits better robustness to spectral interference than the IpDFT algorithm, especially when the oscillating modes are closely spaced in frequency, as it typically occurs when short observation intervals are considered. In addition, the IpDFT algorithm requires a much lower processing burden than the Prony algorithm. Thus, if the observation interval is long enough to ensure an adequate spectral selectivity, the IpDFT algorithm can be advantageously adopted to estimate the modes' parameters of ringdown electromechanical oscillations.

Acknowledgement

This work is supported by the European Union under NextGenerationEU, PRIN 2022 (Prot. no. 20224X2AYH, CUP E53D23000420006).

References

[1] A. Berizzi *et. al*, "Real-time identification of electromechanical oscillations through dynamic mode decomposition," IET Gener. Transm. Distrib., Jul. 2020.

[2] J.C.H. Peng and N.K.C. Nair, "Enhancing Kalman filter for tracking ringdown electromechanical oscillations," IEEE Trans. Power Syst., vol. 27, no. 2, pp. 1042–1050, May 2012.

[3] Estimation of Electromechanical Modes in Power Systems using Synchronized Phasor Measurements and Applications for Control of Inter-Area Oscillations, A contribution to CIGRE WG B5-14 "Wide Area Protection and Control Technologies", Aug. 2013.

[4] A. Messina, Inter-Area Oscillations in Power Systems: A Nonlinear and Nonstationary Perspective. New York: Springer, 2009.

[5] Power System Oscillatory Behaviors: Sources, Characteristics, & Analyses, North American Synchrophasor Initiative (NASPI)-2017-TR-003.

[6] J. F. Hauer, C. J. Demeure, and L. L. Scharf, "Initial results in Prony analysis of power system response signals," IEEE Trans. Power Syst., vol. 5, no. 1, pp. 80–89, Feb. 1990.

[7] D. J. Trudnowski *et al.*, "Making Prony analysis more accurate using multiple signals," IEEE Trans. Power Syst., vol. 14, no. 1, pp. 226–231, Feb. 1999.

[8] M. Netto and L. Milli, "Robust data filtering for estimating electromechanical modes of oscillation via the multichannel Prony method, IEEE Trans. Power Syst., vol. 33, no. 4, pp. 4134–4143, Jul. 2018.

[9] X. Zhang, N. Zhou, X.R. Xie, and Z.Y. Xu, "Performance comparison of three algorithms for estimating oscillation modes using ringdown data," in Proc.: IEEE Power & Energy Society General Meeting, Chicago, USA, 2017.

[10] S. Dekhtiar, P. Chusovitin, and A. Pazderin, "A novel approach for electromechanical mode estimation based on PMU," in Proc.: 9th International Conference on Information Technology and Electrical Engineering (ICITEE), Phuket, Thailand, 2017.

[11] R. A. Wiltshire *et al.*, "A Kalman Filtering approach to rapidly detecting modal changes in power systems," IEEE Trans. Power Syst., vol. 22, no. 4, pp. 1698–1706, Nov. 2007.

[12] J. J. Sanchez-Gasca, Identification of Electromechanical Modes in Power Systems, June 2012.

[13] R. Rane, A. Pandey, and F. Kazi, "Real-time electromechanical mode identification through energy-sorted matrix pencil method," in Proc. 56th International Universities Power Engineering Conference (UPEC), Middlesbrough, UK, 2021.

[14] A. R. Messina and V. Vittal, "Nonlinear, non-stationary analysis of interarea oscillations via Hilbert spectral analysis," IEEE Trans. Power Syst., vol. 21, no. 3, pp. 1234–1241, Aug. 2006.

[15] D. S. Laila, A. R. Messina, and B. C. Pal, "A refined Hilbert–Huang transform with applications to interarea oscillation monitoring," IEEE Trans. Power Syst., vol. 24, no. 2, pp. 610–620, May 2009.

[16] J.A de la O Serna, J.M. Ramirez, A.Z. Mendez, and M.R.A. Paternina, "Identification of electromechanical modes based on the digital Taylor-Fourier transform," IEEE Trans. Instrum. Meas., vol. 31, no. 1, pp. 206-215, Jan. 2016.

[17] H. Zhang, P. Zhang, and X. Wang, "Estimation of inter-area modes during ambient operation using the eigen-system realization algorithm," in Proc: International Conference on Power System Technology: Towards Green, Efficient and Smart Power System, Chengdu, China, 2014, pp. 569–574.

[18] K. Duda, T. P. Zielinski, L. B. Magalas, and M. Majewski, "DFT based estimation of damped oscillation's parameters in low frequency mechanical spectroscopy," IEEE Trans. Instrum. Meas., vol. 60, no. 11, pp. 3608–3618, Nov. 2011.

[19] D. Belega and D. Petri, "Fast interpolated DTFT estimators of frequency and damping factor of real-valued damped sinusoids," Measurement, 2023.

[20] D. Belega and D. Petri, “Frequency and damping factor estimation of real-valued damped sinusoids by means of an improved two-point interpolated DFT algorithm,” Digital Signal Process., vol. 153, Oct. 2024.
[21] A.H. Nuttall, “Some windows with very good sidelobe behavior,” IEEE Acoust., Speech, Signal Process., vol. ASSP-29, no.1, pp 84–91, Feb. 1981.
[22] C. Offelli and D. Petri, “Weigthing effect on the discrete time Fourier transform of noisy signals,” IEEE Trans. Instrum. Meas., vol. 40, no. 6, pp. 972-981, Dec. 1991.
[23] P. Carbone, E. Nunzi, and D. Petri, "Frequency-domain-based least-squares estimation of multifrequency signal parameters," IEEE Trans. on Instr. Meas. vol. 49(3), pp. 555-558, 2000.
[24] D. Belega, D. Petri, and D. Dallet, "Impact of harmonics on the interpolated DFT frequency estimator," Mech. Syst. Signal Proc., vol. 66-67, pp. 349-360, 2016.